Impacts of land cover changes on biogenic emission and its contribution to ozone and secondary organic aerosol in China

Jinlong Ma[1], Shengqiang Zhu[1], Siyu Wang[1], Peng Wang[2,3*], Jianmin Chen[1], Hongliang Zhang[1,3,4*]

[1]Shanghai Key Laboratory of Atmospheric Particle Pollution and Prevention, Department of Environmental Science and Engineering, Fudan University, Shanghai, China
[2]Department of Atmospheric and Oceanic Science, Fudan University, Shanghai 200438, China
[3]IRDR ICoE on Risk Interconnectivity and Governance on Weather/Climate Extremes Impact and Public Health, Fudan University, Shanghai, China

[4]Institute of Eco-Chongming (IEC), Shanghai 200062, China

Correspondence to: Peng Wang (w_peng@fudan.edu.cn); Hongliang Zhang (zhanghl@fudan.edu.cn)

Abstract. The greening impacts in China from 2000 to 2017 led to an increase in vegetated areas and thus enhanced biogenic volatile organic compounds (BVOC) emissions. BVOCs are regarded as important precursors for ozone (O_3) and secondary organic aerosol (SOA). As a result, accurate estimation of BVOC emissions is critical to understanding their impacts on air quality. In this study, Model of Emissions of Gases and Aerosols from Nature (MEGAN) v2.1 was used to investigate the impact of different leaf area index (LAI) and land cover (LC) datasets on BVOC emissions in China in 2016 and the effects on O_3 and SOA were evaluated based on the Community Multiscale Air Quality Modelling System (CMAQ). Three LAI satellite datasets of the Global LAnd Surface Satellite (GLASS), the Moderate Resolution Imaging Spectroradiometer (MODIS) MOD15A2H version 6 (MOD15), and the Copernicus Global Land Service (CGLS), as well as three LC satellite datasets of the MODIS MCD12Q1 LC products, the Copernicus Climate Change Service (C3S) LC products, and the CGLS LC products were used in five parallel experiments (cases: C1-C5). Results show that changing LAI and LC datasets of the model input has an impact on BVOC estimations. BVOC emissions in China range from 25.42 to 37.39 Tg in 2016 and are mainly concentrated in central and south-eastern China, with the highest in C5 (using GLASS and CGLS LC) and the least in C4 (using GLASS and C3S LC). Changing the LC inputs for the MEGAN model has a more significant difference in BVOC estimates than using different LAI datasets. The C4 case has better model performance, indicating that it is the better choice for BVOC estimations in China. Changing the MEGAN inputs further impacts the concentrations of O_3 and SOA. The highest O_3 and biogenic SOA (BSOA) concentrations appear in the C1 (using GLASS and MCD12Q1 LC) simulation, which can reach 12 ppb and 9.8 μg m^{-3}, respectively. Due to the combined effect of local BVOC emissions and the summer monsoon, the relative difference between C1 and C4 is over 52% and 140% in O_3 and BSOA in central and eastern China. The BSOA difference between C1 and C4 is mainly attributed to the isoprene SOA (ISOA), which is a major contributor to BSOA. Particularly, the relative difference in ISOA between these two cases is up to 160% in eastern China. Therefore, our results suggest that the uncertainties in MEGAN inputs should be fully considered in future O_3 and SOA simulations.

1 Introduction

Volatile organic compounds (VOCs) from both natural and anthropogenic sources play important roles in the formation of ozone (O_3) and secondary components of fine particulate matter ($PM_{2.5}$) in addition to their adverse health effects (Volkamer et al., 2006;Laothawornkitkul et al., 2009;Calfapietra et al., 2013;Zhao et al., 2021). Globally, biogenic VOCs from vegetations (BVOCs) are the dominant contributor (with ~90% contribution) to VOCs (Fehsenfeld et al., 1992;Guenther et al., 1995). Isoprene, monoterpenes, and sesquiterpenes are major BVOC species (Guenther et al., 2006;Wang et al., 2018a) with high photo-chemical reactivity with ozone (O_3), hydroxyl radical (OH), and nitrate radical (NO_3). In addition, changes in emissions of BVOCs will alter the capacity of a wide range of warming and cooling climate pollutants, such as O_3, methane (CH_4) and aerosols. O_3 and CH_4 can warm the climate, while the aerosols have a cooling effect by scattering solar radiation (Unger, 2014a, b). Consequently, the studies of BVOC emissions and their effects on air quality and climate are of vital significance.

The Model of Emissions of Gases and Aerosols from Nature (MEGAN) is a widely used (Guenther et al., 2012;Zhao et al., 2016;Emmerson et al., 2018) model to quantify BVOC emissions in different spatial scales (Guenther et al., 1995;Sindelarova et al., 2014;Zhang et al., 2017;Jiang et al., 2019a;Wang et al., 2021). Global annual inventories of the isoprene emission are ranged from 500 to 750 Tg yr^{-1} (Guenther et al., 2006) and those of monoterpene emissions are ranged from 74.4-157 Tg yr^{-1} (Guenther et al., 2012;Messina et al., 2016). BVOC emissions also have been estimated in China by various studies and the results showed that isoprene emissions were 7.17-29.30 Tg yr^{-1} and monoterpene emissions were 2.83-5.60 Tg yr^{-1} (Guenther et al., 2006;Fu and Liao, 2012;Li et al., 2020). The model determined the vegetation types according to model inputs and then use the activity factor multiplied with the emission factor to calculate emissions for each vegetation type (Guenther et al., 2012). However, there are considerable uncertainties in BVOC estimations due to incomplete information on model inputs, activity factors, and emission factors (Situ et al., 2014;Guenther et al., 2012). Those factors can influence the accuracy of estimations and will further result in misunderstanding the impacts on O_3 and SOA. Therefore, it is necessary to quantify the influence of those factors and determine the bias in BVOC emissions.

Land cover (LC), including leaf area index (LAI) and plant function types (PFTs) fractions, is a major factor affecting the BVOC emissions in the MEGAN model (Guenther et al., 2006;Pfister et al., 2008;Guenther et al., 2012). There are many LAI and LC products generated by various satellite sensors with different process methods, spatial and temporal resolutions. These products show discrepancies in biomass distributions and PFTs fractions which can enlarge bias in BVOC estimations (Leung et al., 2010;Wang et al., 2020b;Opacka et al., 2021). Guenther et al. (2006) reported that differences in isoprene emissions could be 24% and 29% due to changing PFTs and LAI, respectively. Pfister et al. (2008) found that differences in BVOC emissions were more significant on a regional scale than global by employing three different PFTs and LAI databases to drive the MEGAN model. Wang et al. (2018a) showed that the differences in BVOC estimations were 35.5% and 22.8% as a result of changing PFTs and LAI, respectively. China is a typical greening country across the world with the forest area of 22.96%

in 2018 (NFGA, 2019), contributing large annual BVOC emissions to the world (Opacka et al., 2021), and thus reasonable comparisons in LAI and LC satellite products are essential for better understanding China BVOC emissions.

Contributions of BVOCs to surface O_3 and SOA have been evaluated through chemical transport models (CTMs) at different spatial scales (Carlton and Baker, 2011;Fu and Liao, 2014;Jiang et al., 2019b;Zhang et al., 2020). Fu and Liao (2012) used the Goddard Earth Observing System chemical transport model (GEOS-Chem) to quantitate the impact of biogenic emissions on O_3 in China over the year 2001-2006 and found that the difference in O_3 concentrations induced by interannual variability of BVOCs could be 2-5%. Based on the Weather Research and Forecasting model coupled with Chemistry (WRF-Chem), Situ et al. (2013) reported that about 57% higher O_3 formed from isoprene in urban areas than in rural areas in the PRD. In addition to the impact on surface O_3, Wu et al. (2020) studied the contributions of BVOCs to SOA in China in 2017 by using the Community Multiscale Air Quality (CMAQ) and the result indicated that BVOCs are the main source of the formation of SOA in summer, which was up to 70%. Qin et al. (2018) investigated the biogenic SOA (BSOA) during summertime in 2012 and found that a high level of BSOA concentration appeared in Sichuan Basin. However, previous studies only focused on the impacts of BVOCs estimated by the specific LAI and LC satellite products on air quality. The uncertainties in BVOC estimations induced by different satellite products also have an impact on O_3 and SOA concentrations. Kim et al. (2014) showed that the different PFTs distributions had a significant impact on hourly and local O_3, which was up to 13 ppb. Wang et al. (2020b) evaluated that the impacts on O_3 reached 20% by using different LC datasets in BVOC emissions in the YRD. The influence of these uncertainties on air quality was not well quantified and the bias in air quality remained unclear in China. Therefore, it is necessary to conduct a comprehensive analysis of the influence of different satellite products on BVOC emissions as well as the further impact on air quality.

In this study, the objectives are to estimate the difference in BVOC emissions induced by different LAI and LC databases in China and study the effects of differences in BVOC emissions on surface O_3 and SOA concentration in China. We used three LAI satellite datasets and three LC satellite datasets as the MEGANv2.1 input to estimate the BVOC emissions and then coupled results with a source-oriented model to quantify the effect on air quality. Section 2 introduces the MEGAN model, the source-oriented CMAQ model, and datasets. The model performance, BVOC estimations based on different satellite products, as well as the impact of BVOCs on atmospheric pollutants are described in Section 3, while Section 4 concludes the study.

2 Methodology

2.1 Model setup

An updated source-oriented CTM was applied to determine O_3 and SOA concentrations from BVOCs based on the CMAQ model v5.0.1 (Byun and Schere, 2006). The model utilizes a revised SAPRC-11 photochemical mechanism (S11) (Carter and Heo, 2013), which includes a more explicit description of isoprene oxidation chemistry to improve isoprene aerosol predictions

(Ying et al., 2015). Changes in the SOA module includes the surface uptake of dicarbonyls and isoprene epoxides, as well as predictions of glyoxal and methylglyoxal (Ying et al., 2015). The aerosol yields are updated to account for vapor wall loss during chamber experiments as described by Zhang et al. (2014). The S11 gas phase mechanism and the SOA module are further expanded with a precursor tracking scheme to track emissions from different sources separately so that the formation of SOA could be determined. The complete description of SOA source tracking has been described by Zhang and Ying (2011) and Wang et al. (2018b), and a brief introduction is described below.

The modified S11 mechanism expands the specific original reactions into two sets of similar reactions to track the formation of O_3 and SOA. The concentrations of O_3 from different VOC sources (henceforth $O_3\_VOC_i$) were determined by the source-oriented method (Ying and Krishnan, 2010). Based on the method, the non-reactive O_3 tracer is used to track O_3 attributed to BVOCs, which is tagged as $O_3\_VOC_{bio}$ and directly predicted. The descriptions of O_3 source apportionment see detailed in Wang et al. (2019). As for SOA, the specific source X (for instance, biogenic source) is tracked by adding a superscript X on the precursors related to SOA (like TERP, the abbreviation of monoterpene in the S11 photochemical mechanism) and their products, while the contributions from all other sources are simulated based on none-tagged TERP. The tagged specie $TERP^x$ reacts with OH to form the primary product $TRPRXN^x$, which is the counter species for aerosol precursor from monoterpenes and subsequently formed semi-volatile oxidation products SV_TRP1^x and SV_TRP2^x based on the two-product approach and thus determines the fine mode SOA species $ATRP1^x$ and $ATRP2^x$ due to gas-to-particle partitioning. By considering those species with the superscript X, it is possible to track the SOA formed by ATRP of source X. The contributions of other precursors of SOA are calculated using the same approach.

The WRF model v3.6.1 was used to generate meteorological conditions for MEGAN and CMAQ. The modelling domain in WRF was 36 km × 36 km in horizontal spatial resolution, which covers China and its surrounding countries in East Asia (Fig. S1) (Zhang et al., 2012). The boundary and initial conditions applied in WRF were from the National Centers for Environmental Prediction (NCEP) Final (FNL) Operational Model Global Tropospheric Analyses dataset (available at http://rda.ucar.edu/datasets/ds083.2/, last access: 18 May 2022). The model configurations are similar to the previous studies (Wang et al., 2018b;Wang et al., 2020a;Zhu et al., 2021) and Table S1 briefly lists the physical options used for the WRF model. The MEGANv2.1 was applied to estimate 19 compound classes of BVOCs (Guenther et al., 2012). In MEGAN, the LC and LAI datasets in 2016 were used and then were gridded to the same spatial resolution to generate PFTs fractions and LAIv maps as inputs for the model. The CMAQ model used the same horizontal resolution as WRF with a horizontal domain of 197 × 127 grid cells. This domain covers China and its surrounding areas (Fig. S1). The meteorological conditions as inputs to CMAQ model were provided by the WRF model v3.6.1. The anthropogenic emissions of China used the datasets from Multiresolution Emission Inventory for China (MEIC; available at http://www. meicmodel.org, last access:3 May 2022). Since the MEIC only provides anthropogenic emissions for China, anthropogenic emissions from foreign countries were provided by the Emissions Database for Global Atmospheric Research (EDGAR) v4.3 (available at http://edgar.jrc.ec.europa.eu/overview.php? v=_431,

last access: 10 May 2022). The MEIC inventory is widely used in air quality studies in China (Li et al., 2017b;Hu et al., 2016;Wu et al., 2020). It had an improvement in a vehicle emission inventory with high resolution (Zheng et al., 2014), and a non-methane VOC mapping approach for different chemical mechanisms (Li et al., 2014). The EDGAR is a grided emissions inventory with a high horizontal resolution of 0.1°×0.1° (Saikawa et al., 2017).

2.2 Data description

LAI and PFTs are key parameters for BVOC estimations. Three LC datasets were applied as PFTs inputs, including the Moderate Resolution Imaging Spectroradiometer (MODIS) MCD12Q1 LC products (Friedl and Sulla-Menashe, 2019), the Copernicus Climate Change Service (C3S) LC products (C3S, 2021), and the Copernicus Global Land Service (CGLS) LC products (Buchhorn et al., 2020). MCD12Q1 provides yearly global LC maps from 2001 to 2020 with spatial resolution at 500 m, which is widely used in previous studies (Guenther et al., 2006;Wang et al., 2018a;Wu et al., 2020). Thus, MCD12Q1 is chosen as the baseline LC input for MEGANv2.1 to investigate the model performance with different LAI satellite products. Sources of these products were listed in Table S2. PFTs used in the MEGAN model adopt the scheme used for Community Land Model v4.0 (CLM4) (Guenther et al., 2012). Three LC maps are first re-gridded to the CMAQ domain (Fig. S2). Secondly, LC types are categorized into eight vegetation types according to legend descriptions of LC maps. Lastly, eight vegetation types are further reclassified into CLM-15 PFTs based on the climate rules described in Bonan et al. (2002). Fig. 1 shows the simulation domain with the spatial distribution of major PFTs. All three datasets represent a similar spatial distribution of grass in northwest China, while there are different PFTs distributing in the central and southern China. Crop land is the dominant PFT in central and southern China in the C3S LC map. Although MCD12Q1 and CGLS LC both show a large area of broadleaf tree in central and southern China, the area fraction of broadleaf tree in CGLS LC is higher than that in MCD12Q1 (Fig 1 and Fig. S3).

The Global LAnd Surface Satellite (GLASS) (Xiao et al., 2014;Xiao et al., 2016), the MODIS MOD15A2H version 6 (MOD15) (Myneni et al., 2015), and the CGLS LAI products (Fuster et al., 2020) were applied as LAI inputs for MEGANv2.1. The spatial resolutions of GLASS, MOD15, and CGLS are 500m, 500m and 300m, respectively, while the temporal resolutions of these three products are 8 days, 8 days, and 10 days, respectively. Sources of these products are listed in Table S2. According to validation results in Xiao et al. (2016), GLASS shows better consistency than MOD15 in high resolution in LAI maps, while CGLS is slightly less accurate than MOD15 (Fuster et al., 2020). Therefore, the GLASS is used as the baseline LAI input. In the MEGAN model, the grid average LAI is divided by the fraction of grid that is covered by vegetation to represent the LAI of vegetation covered surface, which is refer to LAIv (Guenther et al., 2006). Figure 2 represents the spatial distribution of LAI from three satellite datasets in the summer of 2016. The MOD15 LAI dataset used in C2 shows differences from C1, especially in south China where the GLASS LAIv is about 50% higher than the MOD15 LAIv. The MOD15 LAIv is lower in NCP compared to other products, which is because the MOD15 underestimates the LAI of maize and wheat in NCP (Yang et al., 2015;Wang et al., 2022).

Table 1 presents the setup of the simulation scenarios. Scenarios C1 to C3 use MCD12Q1 as the PFTs input and different LAI inputs to investigate the effects of varied LAI datasets on BVOC emissions, while the impacts of different PFTs maps on BVOC estimations are studied in scenarios C1, C4, and C5, which use the GLASS as the LAI input. It should be noted that those experiments use the same meteorological conditions, which are provided by the WRF model, for BVOC estimations. Besides BVOC simulations, a one-year CMAQ simulation with 5 different sets of MEGAN input data is conducted for the year 2016 in China with the same meteorological conditions and anthropogenic emissions to investigate the impacts of BVOCs on O_3 and SOA concentrations. The model chemistry has no effect on meteorological conditions when simulating.

3 Results and discussion

3.1 Model performance

Temperature (T2), relative humidity (RH), wind speed (WS) and wind direction (WD) at 10 m above the surface were compared to observations from the National Climate Data Center (NCDC, available at https://www.ncei.noaa.gov/access, last access: 13 May 2022). The statistical measures and results are shown in Table S3 and Table S4, respectively. T2 predictions are slightly lower than observations in the whole year with negative mean bias (MB) values slightly lower than the benchmarks suggested by Emery et al. (2001). Summer and fall show better performance than spring and winter. It is possible due to the overestimation of cloud coverage in the WRF model leading to an underestimated T2 (Wu et al., 2020). These biases are relatively small compared with previous studies with a yearly long WRF simulation in China (Wu et al., 2020;Wang et al., 2018a). Although the gross error (GE) values of WS are within the criteria of 2 in all seasons, the WRF model still overpredicted the WS. The MB values of WD meet the benchmarks of ±10 in all seasons, but the GE values are over the benchmarks of ±30. In spring and winter, the predicted RH is slightly lower than the observations, while it is overestimated in summer and fall. In addition, the daily variation of temperature was successfully simulated for most cities in China as shown in Fig. S4, and the performance of the WRF model in this study is comparable to previous studies (Hu et al., 2016;Wang et al., 2018a;Wang et al., 2010;Ma et al., 2021). Therefore, the meteorological conditions predicted by the WRF model are acceptable as inputs for the CMAQ model in follow-up research.

Hourly observations from the publishing website of the China National Environmental Monitoring Center (available at http://www.cnemc.cn/, last access: 4 May 2022) were used to validate the CMAQ model prediction of O_3 and $PM_{2.5}$. In order to investigate the impacts of varied total BVOC emissions on main air pollutants, the model performance was evaluated separately for different cases. Table S5 presents the model performance statistics of air pollutants, including maximum daily averaged 1h (MDA1) O_3, maximum daily averaged 8h (MDA8) O_3. The evaluated statistics of mean observations (OBS), mean predictions (PRE), mean fractional bias (MFB), mean fractional error (MFE), mean normalized bias (MNB), and mean normalized error (MNE) were calculated for each case in 2016. Cut-off concentrations of 60 ppb were used for both MDA1

O_3 and MDA8 O_3 in this validation, respectively, which were suggested by the US EPA (EPA, 2005). In general, the model performance on MDA1 O_3 and MDA8 O_3 in all cases in China and its important regions meet the model performance benchmarks suggested by EPA (2005), although the model still overestimates the O_3 concentrations. In China, the MNB value of MDA1 O_3 ranges from 0.02~0.05 and the MNE value of MDA1 O_3 ranges from 0.18~0.19, which are within the criteria of ±0.15 and ±0.3, respectively. In important regions, the MDA1 O_3 concentration in the PRD shows a better consistency with the observations than in the YRD and NCP. The statistical values of MDA1 O_3 in C4 are closer to benchmarks than in the other cases, indicating the better performance of the model simulation of C4. In addition to the comparison of MDA1 O_3, the MNB values of MDA8 O_3 are slightly higher than those of MDA1 O_3, and they also meet the criteria. The MDA8 O_3 in C4 shows better agreement with observations because the statistics are closer to the criteria.

Table S6 presents the model performance statistics on $PM_{2.5}$. The statistical values of $PM_{2.5}$ in all cases are within the criteria (MFB ≤ ±60 % and MFE ≤ 75 %) suggested by Boylan and Russell (2006). However, the predicted $PM_{2.5}$ is slightly lower than the observations, which can be indicated by the negative MFB values. In important regions, the MNB values in the YRD are slightly higher than in other regions, while MFE and MNE values are higher in the PRD. Compared to other cases, the statistical values of $PM_{2.5}$ in C4 are lower, indicating a better performance of $PM_{2.5}$ in C4. Therefore, the BVOC emissions in C4 generated by using C3S LC and GLASS are the best BVOC inventory in this study. Although C1, C2, and C3 adopt LAI satellite products with different accuracies, the accuracies of these products have no significant impact on the model performance due to similar statistics values. The overall statistical values meet the criteria in all cases, which indicates that the O_3 and $PM_{2.5}$ are well captured by the model. Generally, the simulation results of air pollutants in this study are acceptable for the source apportionment study of O_3 and SOA, which was comparable to other studies (Hu et al., 2016;Wu et al., 2020;Liu et al., 2020).

3.2 Simulated BVOC emissions in China

3.2.1 Quantity of BVOC emissions

Table 2 shows the total amount of BVOC emissions and its major components of each case in China in 2016. In general, using different LAI and LC datasets as the MEGAN inputs has an impact on BVOC emissions. Isoprene accounts for the largest share of BVOC emissions with an average of 54% for all cases, and the difference in the isoprene emission of each case is the main reason resulting in the discrepancy in total BVOC emissions between each case. C5 shows the highest BVOC emissions of 37.39 Tg with the isoprene emission of 22.73 Tg, which is also the highest of all cases. In contrast, BVOC emissions of 25.42 Tg and the isoprene emission of 12.1 Tg in C4 both are the lowest in all cases. The BVOC emissions in C1 are about 5 Tg higher than C2. In addition to the impact of LAI datasets on BVOC emissions, the LC dataset used in C4 leads to a 21.4% decrease in the isoprene emission compared to C1, while C5 with the CGLS LC dataset results in an 8% increase in the isoprene emission, which is due to the higher percentage broadleaf tree cover in CGLS LC products (Fig. S3 and Fig. S5). Although

the total BVOC emissions in C5 are 1.29 Tg higher than those in C1, the emissions of monoterpenes, sesquiterpenes, and other VOCs are lower than in C1. This is induced by the discrepancy in the distribution of needleleaf tree and shrubs between C1 and C5, which is in agreement with the result in Wang et al. (2018a) (Fig. S3 and Fig. S5).

3.2.2 Temporal and spatial variation of BVOC emissions

Figure 3 presents the seasonal variations in isoprene, monoterpenes, sesquiterpenes, and total BVOC emissions in all cases in China. In general, using different LAI and LC products does have an impact on the temporal variability in the BVOC emissions. The BVOC emissions show similar seasonal variations in all cases, which are mainly concentrated in summer, accounting for 60.9%-63.8% of total BVOC emissions compared to 2.9%~3.4% in winter. The differences in BVOC emissions between C1 and the other cases are larger when the temperature rises, reaching the maximum in summer, which is because that BVOC emissions are susceptible to the influence of temperature and radiation in the atmosphere (Guenther et al., 2006;Guenther et al., 2012). As the biggest contributor to BVOCs, isoprene emissions can reach 7.94~14.79 Tg in summer. The percentage of winter monoterpenes in the total monoterpenes is higher than that of isoprene and sesquiterpenes, probably because isoprene and sesquiterpenes are more sensitive to temperature changes than monoterpenes (Ibrahim et al., 2010;Bai et al., 2015). C4 used the C3S LC and GLASS shows the lowest emissions in total BVOCs and its main species among each season. Furthermore, the isoprene emission of C5 is the highest among the cases, but the monoterpene and sesquiterpene emissions in C5 are lower than that in C3 as well as in C1, which may be due to the higher distribution of broadleaf trees with the high isoprene EF and lower distribution of grass with the high monoterpene and sesquiterpene EF in CGLS LC compared to those in MCD12Q1.

Since a large proportion of BVOCs is released in summer, which contributes about 62% of total annual emissions, the analysis of the spatial distribution is mainly concentrated on summer BVOC emissions. Figure 4 illustrates the spatial distribution of total BVOCs, isoprene, monoterpenes, and sesquiterpenes during summer in C1 as well as the comparisons between C1 and the other cases. In general, the difference in spatial distribution of BVOCs mainly focuses on central and southeastern China, and the differences induced by different LC products are more significant than by different LAI products. The isoprene, monoterpenes, and sesquiterpenes emissions show similar distribution patterns with hotspots primarily located in the central and southeastern China as shown in Fig. 4 (panels f, k and p). This is due to the high density of tree covers in those regions. Although the GLASS has the same temporal resolution of 8 days as MOD15, differences between the two products still play an important role in impacting the BVOC emissions (Fig. 2 and Fig. 4b). According to Fig. 4 (panels a and q), the difference of emission distribution of isoprene and sesquiterpene between the C1 and C2 is generally consistent with the difference in GLASS and MOD15 in summer (Fig. 2). The changes in the spatial distribution of BVOC emissions in C4 and C5 are more significant compared to C2 and C3. This is because the impacts on BVOC emissions become less when LAIv is greater than 3 (Guenther et al., 2012). The higher emissions of three main BVOC species in the south of China in C1 than in C4 are due to the higher vegetation cover in C1, as shown in Fig. 4 (panels i, n and s). C4 used the C3S LC as the model inputs with crops dominating nearly half of China, and the relatively low EF of the crop for three main BVOC species compared to the other

PFTs, resulting in the lower BVOC estimations in C4 (Fig. 1 and Fig. S5). The spatial distribution of isoprene emission in C5 is conspicuously different than in C1, which is consistent with a difference in the broadleaf tree distribution in the inputs (Fig. S5). Even though C5 shows a higher forest cover than C1 in the north of China, the isoprene emission in C1 is higher than C5 in that place, which is likely due to the difference in the grass distribution and the impact of temperature. Cooler temperatures at higher latitudes inhibit the release of isoprene from forests (Guenther et al., 2006).

3.2.3 Comparison with previous studies

Table 3 illustrates the annual BVOC emissions estimated by MEGAN in China in this study and previous studies. The annual BVOC emissions in this study range from 25.42 ~ 37.39 Tg, which is within the range of 17.30 ~ 54.60 Tg from 2001 to 2018 published in the literatures. BVOC emissions estimated by this study are higher than 18.85 and 23.54 Tg estimated by Fu and Liao (2012), and Wu et al. (2020), respectively. However, results in this study are lower than 58.9 Tg for 2018 estimated by Li et al. (2020). The differences between this study with previous studies can be induced by many factors. The increase in forest coverages may be the main reason for the large difference. According to the reports in National Forest Resources Census, the forest coverages increased relatively about 18.8% from 2003 to 2013 (FGA, 2006, 2014). In addition, the MEGAN inputs as well as algorithms in the model will have an impact on the simulation of BVOC emissions. In this study, the default EFs listed in Guenther et al. (2012) are used for all BVOC species. Fu and Liao (2012) used a set of EFs with 25 PFTs for isoprene and monoterpenes, which are generally lower than the default EFs for MEGAN, leading to much lower BVOC emissions of 18.85 Tg than in this study. Although the same datasets of MODIS MOD15A2H and MODIS MCD12Q1 were used as LAI and PFTs inputs for MEGAN, the estimate in Wu et al. (2020) is lower than in this study due to lower area fractions of the broadleaf tree, which has the highest isoprene EF than other PFTs (Guenther et al., 2012), and absent of area fraction of crop when calculating BVOC emissions for China. There is a considerable difference in BVOC emissions between this study and those of Li et al. (2020). The difference is mainly due to the combined effect of emission rate and PFTs. Liu et al. (2020) produced the basal emission rates for 192 plant species and categorized them into 82 PFTs for China resulting in more BVOC estimates. Besides, the overestimated temperature in Wang et al. (2021) may be the main reason resulting in a higher estimate of 35.48 Tg for 2016 than in our study. In conclusion, uncertainties in the MEGAN simulations can be attributed to these factors in different years, and these uncertainties can lead to significant differences between this study and previous studies. Therefore, the simulated BVOC emissions are within acceptable limits compared to the previous studies.

3.3 Sensitivity of O_3 to BVOC emissions

3.3.1 Spatial distribution of O_3

Figure 5 displays the spatial distribution of MDA1 O_3 and MDA8 O_3 concentration formed by the BVOCs during the summer in C1 as well as the difference between C1 and the other cases. The differences in emissions of BVOCs between C1 and other cases have impacts on the spatial distribution of O_3, and the impacts from changing LC inputs are greater than that from

changing LAI inputs. The O_3 concentration hotspots are mainly concentrated in central and eastern China, where MDA1 O_3 concentrations can reach more than 12 ppb in C1. This is possibly due to the combine effect of BVOC emissions and Asian summer monsoon. The Asian summer monsoon brings in oceanic air masses with low O_3 concentrations and transports O_3 from southern to central and northern China (Zhao et al., 2010;Li et al., 2018). As shown in Fig. 5d, the spatial distribution of O_3 concentration in C4 is different than in C1, especially in central and eastern China, where the relative difference is over 52%. Although C5 has higher BVOC emissions than C1 in southern China, it does not have much impact on O_3 formation (Fig. 4), which is possibly due to the effect of O_3-NO_x-VOC sensitivity. According to the study of Jin and Holloway (2015) , these regions belong to NO_x-limited regions, in which NO_x is limited but VOCs are abundant, and thus the higher BVOC emissions have few impacts on the formation of O_3. In contrast, the areas with low VOCs emissions will contribute more to the O_3 formation when VOCs emissions increase, such as in the NCP and YRD. MDA8 O_3 shows a similar spatial distribution pattern to MDA1 O_3 in C1, but the concentration is 3-6 ppb lower than that of MDA1 O_3.

3.3.2 Temporal distribution of O_3

Figure 6 illustrates the contribution of BVOC emissions to MDA1 O_3 and MDA8 O_3 in important regions and China in different seasons. In general, the differences of O_3 concentration between each case show seasonal variations in China and are significant in summer. O_3 concentrations formed by the biogenic source are high in summer and low in winter, which is due to the combined effect of BVOC emissions and wind. The summer monsoon transports a large amount of O_3 from southern China to the YRD and NCP (Zhao et al., 2010), resulting in a large difference in O_3 concentrations between different cases. C1, C3, and C5 have a similar O_3 concentration in each season due to the similar BVOC emissions. In the YRD, the MDA1 O_3 in C1 is 78% higher than in C4, which is due to the effect of O_3-NO_x-VOC sensitivity. Higher BVOC emissions in VOC-limited regions lead to the higher O_3 formation (Jin and Holloway, 2015). In most areas of China, especially in the YRD and NCP, the discrepancies between each case are expanded with the increase of the biogenic O_3 concentration, which indicates that seasonal variations of BVOC emissions have an impact on the differences between each case. Besides, the wind effect also plays an important role in seasonal variations of O_3 concentrations (Fig. S6), especially in the PRD. The clean oceanic air masses are brought by the wind to the southeast of China resulting in a decrease in local O_3 concentrations (Zhao et al., 2010). However, the wind in fall transports heavy pollutants from northern to southern China, increasing the O_3 concentrations in southern China (Li et al., 2018). Therefore, the seasonal variations of O_3 and differences in O_3 concentrations between each case are not significant in the PRD due to the combine effect of wind and temperature (Table S7). In all cases, MDA8 O_3 shows a similar temporal distribution to MDA1 O_3 in China and important regions, but the fall contribution is lower than the spring contribution, which is the opposite of MDA1 O_3.

3.4 Sensitivity of SOA to BVOC emissions

3.4.1 Spatial distribution of SOA and components

Figure 7 presents the spatial distribution of BSOA during the summer in C1 as well as the difference between C1 and other cases. In general, using different LC datasets as MEGAN inputs shows more significant impacts on SOA formation. The hotspots of BSOA are mainly concentrated in central and eastern China, especially in Sichuan Basin (Fig. S1), where the BSOA concentration is up to 9.8 μg m^{-3}. This is because that the high surface wind brings the BSOA from southern China to central China and then, low wind speeds and the topography condition in Sichuan Basin, which are against the pollutant diffusion, result in accumulation of BSOA (Li et al., 2017a). The differences in BSOA concentrations between C1 and C2 are inconspicuous due to the slightly change in BVOCs between them. In contrast, the LC inputs show higher impacts on BSOA concentrations. According to Fig. 7d, the difference in the BSOA concentration between C1 and C4 is conspicuous, especially in central and eastern China, where the relative difference is over 140% in summer. The spatial distribution of BSOA differences between C1 and C5 is similar to the spatial distribution of isoprene emission differences between them, suggesting that BSOA concentrations are more sensitive to isoprene emission than monoterpenes and sesquiterpenes. Considering the share of BSOA in the total SOA concentration in summer, the difference in BVOC emissions due to changing the MEGAN inputs can therefore have a significant impact on SOA concentrations estimated by CMAQ.

Figure 8 displays the spatial distribution of SOA formed by isoprene (ISOA), monoterpenes (MSOA) and sesquiterpenes (SSOA) during summer in C1 as well as the difference between C1 and the other cases. The ISOA, MSOA and SSOA show a similar spatial distribution for all cases in China. According to Fig. 8 (panels a, b and c), the high SOA concentration from these three BVOC species mainly concentrated in central and eastern China. This phenomenon is likely due to the combined effect of BVOC emissions and meteorological conditions in these areas. A large amount of SOA is generated in southern China and then transported to central and eastern China due to wind effects in summer. The ISOA is the most important contributor to BSOA, which is 1 time higher than MSOA and 1.5 times higher than SSOA. Comparing C1 with other cases, the difference in the ISOA concentration basically shows a certain correlation with the difference in BVOCs (Fig. 4). The relative difference in ISOA concentrations between C1 and C4 can reach 160% in eastern China, which is higher than that in MSOA and SSOA. This can be attributed to the large discrepancy in their isoprene emission (Fig.8j, k, and l). The ISOA concentrations in southeastern China are lower in C1 than in C5, but the MSOA and SSOA concentrations are higher than in C5, which is due to the difference in BVOC estimations between them. Changing the MEGAN inputs has a large impact on isoprene emissions, which are the main contributor to BVOC emissions. This further impact the formation of SOA.

3.4.2 Temporal distribution of SOA

Figure 9 illustrates the seasonal variation in biogenic SOA (BSOA) concentrations in China and the important regions for all cases. In general, the differences in BSOA concentrations between each case are more significant in summer than in other

seasons. The BSOA concentration follows the seasonal cycle of summer > spring > fall > winter in China, NCP as well as YRD. However, the higher BSOA concentration in the PRD occurs in spring, which is due to changes in the wind direction from the erratic wind in spring to the southerly wind in summer (Fig. S7). There are slight differences in BSOA concentrations between C1, C3 and C5 in China, while the differences in C2 and C4 are more conspicuous, especially in the YRD, in which the summer BSOA in C1 is 2.5 times higher than that in C4. This is because that the summer BVOC emissions in C1 are higher than those in C4 in the YRD (Fig. S8) and thus formed more BSOA. The BSOA in C1 is higher than C5 in most areas of China except for the PRD, which is due to the higher isoprene emission in C5 in the PRD (Fig. 4).

4 Conclusion

In this study, we used the different LAI and LC datasets as the MEGAN inputs to estimate the BVOC emissions in 2016 over China and then utilized the WRF-CMAQ model to quantify the contribution of BVOCs to O_3 and SOA concentrations. Besides, the impact induced by those inputs on O_3 and SOA formation was also evaluated. Five experiments were conducted based on three LAI satellite products (GLASS, MOD15, and CGLS) and three LC satellite products (MCD12Q1, C3S, and CGLS). According to model validations, C4 with GLASS and C3S LC was the better choice for China BVOC estimations compared to other scenarios. BVOC emissions in China ranged from 25.42 to 37.39 Tg in 2016 and were mainly concentrated in central and southeastern China, which was due to the high density of tree covers in those regions. In comparison with LAI inputs, using different LC satellite products had a more significant impact on BVOC emissions.

The O_3 formed by BVOCs were mainly concentrated in central and eastern China, where O_3 concentrations could reach 12 ppb. This was possibly due to the combine effect of BVOC emissions and summer monsoon. According to the sensitivity analysis, C1 contributed most to the summer O_3, which was 78% higher than C4 in the YRD. The BSOA were also concentrated in central and eastern China, especially in Sichuan Basin, where the BSOA concentration was up to 9.8 $\mu g\ m^{-3}$. The differences in BSOA concentrations between C1 and C2 are inconspicuous due to the slightly change in BVOCs induced by LAI inputs. In contrast, the LC inputs show higher impacts on BSOA concentrations. This is the same to O_3. Therefore, changing LAI and LC datasets of the model input has an impact on O_3 and SOA formation, where the LC shows more pronounced effect than LAI. Our results suggest that the uncertainties in MEGAN inputs should be carefully considered in future O_3 and SOA simulations.

From 2000 to 2017, global leaf area of vegetation increased by 6.6% due to the direct land-use management, which may also enhance BVOC emissions, leading to further effects on air quality. Thus, the findings of this study can be extended to other regions and global scales, suggesting an urgent need to construct a reliable BVOC emission inventory for local and global scales, and evaluate their impacts on air quality. However, the limitation of observed data of BVOCs and organic components impedes the construction of the accurate emission inventory. Therefore, filed measurements are needed to provide more data for model validations. In addition, urban BVOC emissions play important roles in urban air quality, it would be interesting to study the impact of biogenic sources on the urban air quality by using high resolution LC satellite maps.

Author contributions. JM conducted the modelling and write the paper. SZ and SW assisted with data analysis. PW and HZ designed the study, discussed the results, and edited the paper.

Competing interests. The authors declare that they have no conflict of interest.

Financial support. The DFG-NSFC Sino-German AirChanges project (448720203), National Natural Science Foundation of China (42077194/42061134008), and Shanghai International Science and Technology Partnership Project (No. 21230780200) funded this work.

References

Bai, J., Guenther, A., Turnipseed, A., and Duhl, T.: Seasonal and interannual variations in whole-ecosystem isoprene and monoterpene emissions from a temperate mixed forest in Northern China, Atmospheric Pollution Research, 6, 696-707, https://doi.org/10.5094/APR.2015.078, 2015.

Boylan, J. W., and Russell, A. G.: PM and light extinction model performance metrics, goals, and criteria for three-dimensional air quality models, Atmos. Environ., 40, 4946-4959, https://doi.org/10.1016/j.atmosenv.2005.09.087, 2006.

Buchhorn, M., Smets, B., Bertels, L., DeRoo, B., Lesiv, M., Tsendbazar, N.-E., Herold, M., and Fritz, S.: Copernicus Global Land Service: Land Cover 100m: collection 3: epoch 2019: Globe (V3.0.1) [Data set], Zenodo, https://doi.org/10.5281/zenodo.3939050, 2020.

Byun, D., and Schere, K. L.: Review of the Governing Equations, Computational Algorithms, and Other Components of the Models-3 Community Multiscale Air Quality (CMAQ) Modeling System, Appl. Mech. Rev., 59, 51-77, 10.1115/1.2128636, 2006.

C3S: Product User Guide and Specification, 2021.

Calfapietra, C., Fares, S., Manes, F., Morani, A., Sgrigna, G., and Loreto, F.: Role of Biogenic Volatile Organic Compounds (BVOC) emitted by urban trees on ozone concentration in cities: A review, Environ. Pollut., 183, 71-80, 10.1016/j.envpol.2013.03.012, 2013.

Carlton, A. G., and Baker, K. R.: Photochemical Modeling of the Ozark Isoprene Volcano: MEGAN, BEIS, and Their Impacts on Air Quality Predictions, Environ. Sci. Technol., 45, 4438-4445, 10.1021/es200050x, 2011.

Carter, W. P. L., and Heo, G.: Development of revised SAPRC aromatics mechanisms, Atmos. Environ., 77, 404-414, https://doi.org/10.1016/j.atmosenv.2013.05.021, 2013.

Emery, C., Tai, E., and Yarwood, G.: Enhanced meteorological modeling and performance evaluation for two texas episodes, Report to the Texas Natural Resources Conservation Commission, prepared by ENVIRON, International Corp., Novato, CA, 2001.

Emmerson, K. M., Cope, M. E., Galbally, I. E., Lee, S., and Nelson, P. F.: Isoprene and monoterpene emissions in south-east Australia: comparison of a multi-layer canopy model with MEGAN and with atmospheric observations, Atmos. Chem. Phys., 18, 7539-7556, 10.5194/acp-18-7539-2018, 2018.

EPA, U. S.: Guidance on the Use of Models and Other Analyses in Attainment Demonstrations for the 8-hour Ozone NAAQS, EPA-454/R-05-002, 2005.

Fehsenfeld, F., Calvert, J., Fall, R., Goldan, P., Guenther, A. B., Hewitt, C. N., Lamb, B., Liu, S., Trainer, M., Westberg, H., and Zimmerman, P.: Emissions of volatile organic compounds from vegetation and the implications for atmospheric chemistry, Global Biogeochem Cycles., 6, 389-430, https://doi.org/10.1029/92GB02125, 1992.

The Sixth National Forest Resources Inventory: http://www.forestry.gov.cn/portal/main/s/65/content-90.html, 2006.

FGA, C.: The Eighth National Forest Resources Inventory, 2014.

Friedl, M., and Sulla-Menashe, D.: MCD12Q1 MODIS/Terra+Aqua Land Cover Type Yearly L3 Global 500m SIN Grid V006 [Data set], NASA EOSDIS Land Processes DAAC, https://doi.org/10.5067/MODIS/MCD12Q1.006, 2019.

Fu, Y., and Liao, H.: Simulation of the interannual variations of biogenic emissions of volatile organic compounds in China: Impacts on tropospheric ozone and secondary organic aerosol, Atmos. Environ., 59, 170-185, https://doi.org/10.1016/j.atmosenv.2012.05.053, 2012.

Fu, Y., and Liao, H.: Impacts of land use and land cover changes on biogenic emissions of volatile organic compounds in China from the late 1980s to the mid-2000s: implications for tropospheric ozone and secondary organic aerosol, Tellus B., 66, 10.3402/tellusb.v66.24987, 2014.

Fuster, B., Sánchez-Zapero, J., Camacho, F., García-Santos, V., Verger, A., Lacaze, R., Weiss, M., Baret, F., and Smets, B.: Quality Assessment of PROBA-V LAI, fAPAR and fCOVER Collection 300 m Products of Copernicus Global Land Service, Remote Sens., 12, 10.3390/rs12061017, 2020.

Guenther, A., Hewitt, C. N., Erickson, D., Fall, R., Geron, C., Graedel, T., Harley, P., Klinger, L., Lerdau, M., McKay, W. A., Pierce, T., Scholes, B., Steinbrecher, R., Tallamraju, R., Taylor, J., and Zimmerman, P.: A global model of natural volatile organic compound emissions, J. Geophys. Res. Atmos., 100, 8873-8892, https://doi.org/10.1029/94JD02950, 1995.

Guenther, A., Karl, T., Harley, P., Wiedinmyer, C., Palmer, P. I., and Geron, C.: Estimates of global terrestrial isoprene emissions using MEGAN (Model of Emissions of Gases and Aerosols from Nature), Atmos. Chem. Phys., 6, 3181-3210, 10.5194/acp-6-3181-2006, 2006.

Guenther, A. B., Jiang, X., Heald, C. L., Sakulyanontvittaya, T., Duhl, T., Emmons, L. K., and Wang, X.: The Model of Emissions of Gases and Aerosols from Nature version 2.1 (MEGAN2.1): an extended and updated framework for modeling biogenic emissions, Geosci. Model Dev., 5, 1471-1492, 10.5194/gmd-5-1471-2012, 2012.

Hu, J., Chen, J., Ying, Q., and Zhang, H.: One-year simulation of ozone and particulate matter in China using WRF/CMAQ modeling system, Atmos. Chem. Phys., 16, 10333-10350, 10.5194/acp-16-10333-2016, 2016.

Ibrahim, M. A., Maenpaa, M., Hassinen, V., Kontunen-Soppela, S., Malec, L., Rousi, M., Pietikainen, L., Tervahauta, A., Karenlampi, S., Holopainen, J. K., and Oksanen, E. J.: Elevation of night-time temperature increases terpenoid emissions from Betula pendula and Populus tremula, J Exp Bot, 61, 1583-1595, 10.1093/jxb/erq034, 2010.

Jiang, J., Aksoyoglu, S., Ciarelli, G., Oikonomakis, E., El-Haddad, I., Canonaco, F., O'Dowd, C., Ovadnevaite, J., Cruz Minguillon, M., Baltensperger, U., and Prevot, A. S. H.: Effects of two different biogenic emission models on modelled ozone and aerosol concentrations in Europe, Atmos. Chem. Phys., 19, 3747-3768, 10.5194/acp-19-3747-2019, 2019a.

Jiang, J. H., Aksoyoglu, S., Ciarelli, G., Oikonomakis, E., El-Haddad, I., Canonaco, F., O'Dowd, C., Ovadnevaite, J., Minguillon, M. C., Baltensperger, U., and Prevot, A. S. H.: Effects of two different biogenic emission models on modelled ozone and aerosol concentrations in Europe, Atmos. Chem. Phys., 19, 3747-3768, 10.5194/acp-19-3747-2019, 2019b.

Jin, X., and Holloway, T.: Spatial and temporal variability of ozone sensitivity over China observed from the Ozone Monitoring Instrument, J. Geophys. Res. Atmos., 120, 7229-7246, https://doi.org/10.1002/2015JD023250, 2015.

Kim, H. K., Woo, J. H., Park, R. S., Song, C. H., Kim, J. H., Ban, S. J., and Park, J. H.: Impacts of different plant functional types on ambient ozone predictions in the Seoul Metropolitan Areas (SMAs), Korea, Atmos. Chem. Phys., 14, 7461-7484, 10.5194/acp-14-7461-2014, 2014.

Laothawornkitkul, J., Taylor, J. E., Paul, N. D., and Hewitt, C. N.: Biogenic Volatile Organic Compounds in the Earth System, New Phytol., 183, 27-51, 2009.

Leung, D. Y. C., Wong, P., Cheung, B. K. H., and Guenther, A.: Improved land cover and emission factors for modeling biogenic volatile organic compounds emissions from Hong Kong, Atmos. Environ., 44, 1456-1468, 10.1016/j.atmosenv.2010.01.012, 2010.

Li, J., Zhang, M., Wu, F., Sun, Y., and Tang, G.: Assessment of the impacts of aromatic VOC emissions and yields of SOA on SOA concentrations with the air quality model RAMS-CMAQ, Atmos. Environ., 158, 105-115, https://doi.org/10.1016/j.atmosenv.2017.03.035, 2017a.

Li, L., Yang, W., Xie, S., and Wu, Y.: Estimations and uncertainty of biogenic volatile organic compound emission inventory in China for 2008–2018, Sci. Total. Environ., 733, 139301, https://doi.org/10.1016/j.scitotenv.2020.139301, 2020.

Li, L. Y., Chen, Y., and Xie, S. D.: Spatio-temporal variation of biogenic volatile organic compounds emissions in China, Environ. Pollut., 182, 157-168, https://doi.org/10.1016/j.envpol.2013.06.042, 2013.

Li, M., Zhang, Q., Streets, D. G., He, K. B., Cheng, Y. F., Emmons, L. K., Huo, H., Kang, S. C., Lu, Z., Shao, M., Su, H., Yu, X., and Zhang, Y.: Mapping Asian anthropogenic emissions of non-methane volatile organic compounds to multiple chemical mechanisms, Atmos. Chem. Phys., 14, 5617-5638, 10.5194/acp-14-5617-2014, 2014.

Li, M., Liu, H., Geng, G., Hong, C., Liu, F., Song, Y., Tong, D., Zheng, B., Cui, H., Man, H., Zhang, Q., and He, K.: Anthropogenic emission inventories in China: a review, National Science Review, 4, 834-866, 10.1093/nsr/nwx150, 2017b.

Li, S., Wang, T., Huang, X., Pu, X., Li, M., Chen, P., Yang, X.-Q., and Wang, M.: Impact of East Asian Summer Monsoon on Surface Ozone Pattern in China, J. Geophys. Res. Atmos., 123, 1401-1411, https://doi.org/10.1002/2017JD027190, 2018.

Liu, J., Shen, J., Cheng, Z., Wang, P., Ying, Q., Zhao, Q., Zhang, Y., Zhao, Y., and Fu, Q.: Source apportionment and regional transport of anthropogenic secondary organic aerosol during winter pollution periods in the Yangtze River Delta, China, Sci. Total. Environ., 710, 135620, https://doi.org/10.1016/j.scitotenv.2019.135620, 2020.

Ma, J., Shen, J., Wang, P., Zhu, S., Wang, Y., Wang, P., Wang, G., Chen, J., and Zhang, H.: Modeled changes in source contributions of particulate matter during the COVID-19 pandemic in the Yangtze River Delta, China, Atmos. Chem. Phys., 21, 7343-7355, 10.5194/acp-21-7343-2021, 2021.

Messina, P., Lathière, J., Sindelarova, K., Vuichard, N., Granier, C., Ghattas, J., Cozic, A., and Hauglustaine, D. A.: Global biogenic volatile organic compound emissions in the ORCHIDEE and MEGAN models and sensitivity to key parameters, Atmos. Chem. Phys., 16, 14169-14202, 10.5194/acp-16-14169-2016, 2016.

Myneni, R. B., Knyazikhin, Y., and Park, T.: MOD15A2H MODIS/Terra Leaf Area Index/FPAR 8-Day L4 Global 500m SIN Grid V006 [Data set], NASA EOSDIS Land Processes DAAC, https://doi.org/10.5067/MODIS/MOD15A2H.006, 2015.

NFGA: China Forest Resources Report (2014-2018), 1 ed., China Forestry Press, 2019.

Opacka, B., Muller, J.-F., Stavrakou, T., Bauwens, M., Sindelarova, K., Markova, J., and Guenther, A. B.: Global and regional impacts of land cover changes on isoprene emissions derived from spaceborne data and the MEGAN model, Atmos. Chem. Phys., 21, 8413-8436, 10.5194/acp-21-8413-2021, 2021.

Pfister, G. G., Emmons, L. K., Hess, P. G., Lamarque, J. F., Orlando, J. J., Walters, S., Guenther, A., Palmer, P. I., and Lawrence, P. J.: Contribution of isoprene to chemical budgets: A model tracer study with the NCAR CTM MOZART-4, J. Geophys. Res. Atmos., 113, https://doi.org/10.1029/2007JD008948, 2008.

Qin, M., Wang, X., Hu, Y., Ding, X., Song, Y., Li, M., Vasilakos, P., Nenes, A., and Russell, A. G.: Simulating Biogenic Secondary Organic Aerosol During Summertime in China, J. Geophys. Res. Atmos., 123, 11,100-111,119, https://doi.org/10.1029/2018JD029185, 2018.

Saikawa, E., Kim, H., Zhong, M., Avramov, A., Zhao, Y., Janssens-Maenhout, G., Kurokawa, J. I., Klimont, Z., Wagner, F., Naik, V., Horowitz, L. W., and Zhang, Q.: Comparison of emissions inventories of anthropogenic air pollutants and greenhouse gases in China, Atmos. Chem. Phys., 17, 6393-6421, 10.5194/acp-17-6393-2017, 2017.

Sindelarova, K., Granier, C., Bouarar, I., Guenther, A., Tilmes, S., Stavrakou, T., Muller, J. F., Kuhn, U., Stefani, P., and Knorr, W.: Global data set of biogenic VOC emissions calculated by the MEGAN model over the last 30 years, Atmos. Chem. Phys., 14, 9317-9341, 10.5194/acp-14-9317-2014, 2014.

Situ, S., Guenther, A., Wang, X., Jiang, X., Turnipseed, A., Wu, Z., Bai, J., and Wang, X.: Impacts of seasonal and regional variability in biogenic VOC emissions on surface ozone in the Pearl River delta region, China, Atmos. Chem. Phys., 13, 11803-11817, 10.5194/acp-13-11803-2013, 2013.

Situ, S., Wang, X., Guenther, A., Zhang, Y., Wang, X., Huang, M., Fan, Q., and Xiong, Z.: Uncertainties of isoprene emissions in the MEGAN model estimated for a coniferous and broad-leaved mixed forest in Southern China, Atmos. Environ., 98, 105-110, https://doi.org/10.1016/j.atmosenv.2014.08.023, 2014.

Stavrakou, T., Müller, J. F., Bauwens, M., De Smedt, I., Van Roozendael, M., Guenther, A., Wild, M., and Xia, X.: Isoprene emissions over Asia 1979-2012: impact of climate and land-use changes, Atmos. Chem. Phys., 14, 4587-4605, 10.5194/acp-14-4587-2014, 2014.

Unger, N.: On the role of plant volatiles in anthropogenic global climate change, Geophys. Res. Lett., 41, 8563-8569, 10.1002/2014GL061616, 2014a.

Unger, N.: Human land-use-driven reduction of forest volatiles cools global climate, Nat. Clim. Change, 4, 907-910, 10.1038/nclimate2347, 2014b.

Volkamer, R., Jimenez, J. L., San Martini, F., Dzepina, K., Zhang, Q., Salcedo, D., Molina, L. T., Worsnop, D. R., and Molina, M. J.: Secondary organic aerosol formation from anthropogenic air pollution: Rapid and higher than expected, Geophys. Res. Lett., 33, 10.1029/2006GL026899, 2006.

Wang, H., Wu, Q., Liu, H., Wang, Y., Cheng, H., Wang, R., Wang, L., Xiao, H., and Yang, X.: Sensitivity of biogenic volatile organic compound emissions to leaf area index and land cover in Beijing, Atmos. Chem. Phys., 18, 9583-9596, 10.5194/acp-18-9583-2018, 2018a.

Wang, H., Wu, Q., Guenther, A. B., Yang, X., Wang, L., Xiao, T., Li, J., Feng, J., Xu, Q., and Cheng, H.: A long-term estimation of biogenic volatile organic compound (BVOC) emission in China from 2001–2016: the roles of land cover change and climate variability, Atmos. Chem. Phys., 21, 4825-4848, 10.5194/acp-21-4825-2021, 2021.

Wang, L., Jang, C., Zhang, Y., Wang, K., Zhang, Q., Streets, D., Fu, J., Lei, Y., Schreifels, J., He, K., Hao, J., Lam, Y.-F., Lin, J., Meskhidze, N., Voorhees, S., Evarts, D., and Phillips, S.: Assessment of air quality benefits from national air pollution control policies in China. Part I: Background, emission scenarios and evaluation of meteorological predictions, Atmos. Environ., 44, 3442-3448, https://doi.org/10.1016/j.atmosenv.2010.05.051, 2010.

Wang, P., Ying, Q., Zhang, H., Hu, J., Lin, Y., and Mao, H.: Source apportionment of secondary organic aerosol in China using a regional source-oriented chemical transport model and two emission inventories, Environ. Pollut., 237, 756-766, https://doi.org/10.1016/j.envpol.2017.10.122, 2018b.

Wang, P., Chen, Y., Hu, J., Zhang, H., and Ying, Q.: Source apportionment of summertime ozone in China using a source-oriented chemical transport model, Atmos. Environ., 211, 79-90, https://doi.org/10.1016/j.atmosenv.2019.05.006, 2019.

Wang, P., Chen, K., Zhu, S., Wang, P., and Zhang, H.: Severe air pollution events not avoided by reduced anthropogenic activities during COVID-19 outbreak, Resources, Conservation and Recycling, 158, 104814, https://doi.org/10.1016/j.resconrec.2020.104814, 2020a.

Wang, R., Bei, N., Wu, J., Li, X., Liu, S., Yu, J., Jiang, Q., Tie, X., and Li, G.: Cropland nitrogen dioxide emissions and effects on the ozone pollution in the North China plain, Environ. Pollut., 294, 118617, https://doi.org/10.1016/j.envpol.2021.118617, 2022.

Wang, Y., Zhao, Y., Zhang, L., Zhang, J., and Liu, Y.: Modified regional biogenic VOC emissions with actual ozone stress and integrated land cover information: A case study in Yangtze River Delta, China, Sci. Total. Environ., 727, 10.1016/j.scitotenv.2020.138703, 2020b.

Wu, K., Yang, X., Chen, D., Gu, S., Lu, Y., Jiang, Q., Wang, K., Ou, Y., Qian, Y., Shao, P., and Lu, S.: Estimation of biogenic VOC emissions and their corresponding impact on ozone and secondary organic aerosol formation in China, Atmos. Res., 231, 104656, https://doi.org/10.1016/j.atmosres.2019.104656, 2020.

Xiao, Z., Liang, S., Wang, J., Chen, P., Yin, X., Zhang, L., and Song, J.: Use of General Regression Neural Networks for Generating the GLASS Leaf Area Index Product From Time-Series MODIS Surface Reflectance, IEEE Trans Geosci. Remote Sens., 52, 209-223, 10.1109/TGRS.2013.2237780, 2014.

Xiao, Z., Liang, S., Wang, J., Xiang, Y., Zhao, X., and Song, J.: Long-Time-Series Global Land Surface Satellite Leaf Area Index Product Derived From MODIS and AVHRR Surface Reflectance, IEEE Trans Geosci. Remote Sens., 54, 5301-5318, 10.1109/TGRS.2016.2560522, 2016.

Yang, F., Yang, J., Wang, J., and Zhu, Y.: Assessment and Validation of MODIS and GEOV1 LAI With Ground-Measured Data and an Analysis of the Effect of Residential Area in Mixed Pixel, IEEE Journal of Selected Topics in Applied Earth Observations and Remote Sensing, 8, 763-774, 10.1109/JSTARS.2014.2340452, 2015.

Ying, Q., and Krishnan, A.: Source contributions of volatile organic compounds to ozone formation in southeast Texas, J. Geophys. Res. Atmos., 115, https://doi.org/10.1029/2010JD013931, 2010.

Ying, Q., Li, J., and Kota, S. H.: Significant Contributions of Isoprene to Summertime Secondary Organic Aerosol in Eastern United States, Environ. Sci. Technol., 49, 7834-7842, 10.1021/acs.est.5b02514, 2015.

Zhang, H., and Ying, Q.: Secondary organic aerosol formation and source apportionment in Southeast Texas, Atmos. Environ., 45, 3217-3227, https://doi.org/10.1016/j.atmosenv.2011.03.046, 2011.

Zhang, H., Li, J., Ying, Q., Yu, J. Z., Wu, D., Cheng, Y., He, K., and Jiang, J.: Source apportionment of $PM_{2.5}$ nitrate and sulfate in China using a source-oriented chemical transport model, Atmos. Environ., 62, 228-242, https://doi.org/10.1016/j.atmosenv.2012.08.014, 2012.

Zhang, R., Cohan, A., Biazar, A. P., and Cohan, D. S.: Source apportionment of biogenic contributions to ozone formation over the United States, Atmos. Environ., 164, 8-19, 10.1016/j.atmosenv.2017.05.044, 2017.

Zhang, X., Cappa, C. D., Jathar, S. H., McVay, R. C., Ensberg, J. J., Kleeman, M. J., and Seinfeld, J. H.: Influence of vapor wall loss in laboratory chambers on yields of secondary organic aerosol, Proc. Nat. Acad. Sci., 111, 5802-5807, 10.1073/pnas.1404727111, 2014.

Zhang, Y. L., Zhang, R. X., Yu, J. Z., Zhang, Z., Yang, W. Q., Zhang, H. N., Lyu, S. J., Wang, Y. S., Dai, W., Wang, Y. H., and Wang, X. M.: Isoprene Mixing Ratios Measured at Twenty Sites in China During 2012-2014: Comparison With Model Simulation, J. Geophys. Res. Atmos., 125, 10.1029/2020JD033523, 2020.

Zhao, C., Wang, Y., Yang, Q., Fu, R., Cunnold, D., and Choi, Y.: Impact of East Asian summer monsoon on the air quality over China: View from space, Journal of Geophysical Research: Atmospheres, 115, https://doi.org/10.1029/2009JD012745, 2010.

Zhao, C., Huang, M. Y., Fast, J. D., Berg, L. K., Qian, Y., Guenther, A., Gu, D. S., Shrivastava, M., Liu, Y., Walters, S., Pfister, G., Jin, J. M., Shilling, J. E., and Warneke, C.: Sensitivity of biogenic volatile organic compounds to land surface parameterizations and vegetation distributions in California, Geosci. Model Dev., 9, 1959-1976, 10.5194/gmd-9-1959-2016, 2016.

Zhao, H., Chen, K., Liu, Z., Zhang, Y., Shao, T., and Zhang, H.: Coordinated control of PM2.5 and O3 is urgently needed in China after implementation of the "Air pollution prevention and control action plan", Chemosphere, 270, 129441, https://doi.org/10.1016/j.chemosphere.2020.129441, 2021.

Zheng, B., Huo, H., Zhang, Q., Yao, Z. L., Wang, X. T., Yang, X. F., Liu, H., and He, K. B.: High-resolution mapping of vehicle emissions in China in 2008, Atmos. Chem. Phys., 14, 9787-9805, 10.5194/acp-14-9787-2014, 2014.

Zhu, S., Poetzscher, J., Shen, J., Wang, S., Wang, P., and Zhang, H.: Comprehensive Insights Into O3 Changes During the COVID-19 From O3 Formation Regime and Atmospheric Oxidation Capacity, Geophys. Res. Lett., 48, e2021GL093668, https://doi.org/10.1029/2021GL093668, 2021.

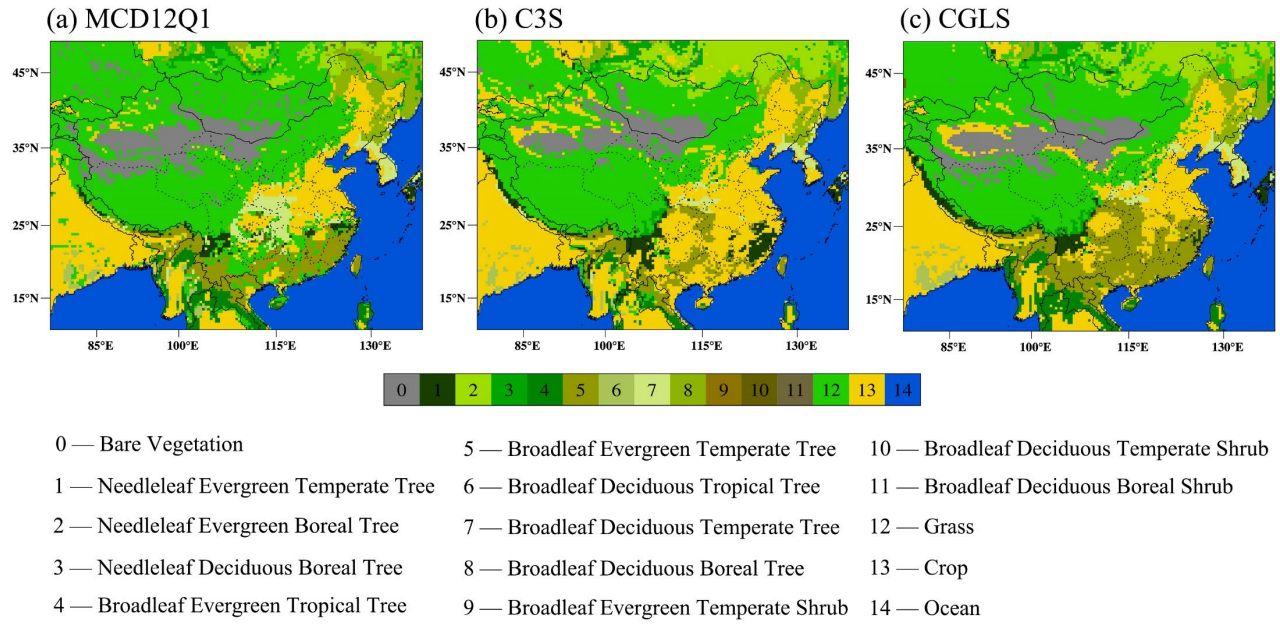

Figure 1. Simulation domain with the spatial distribution of major PFTs in each grid.

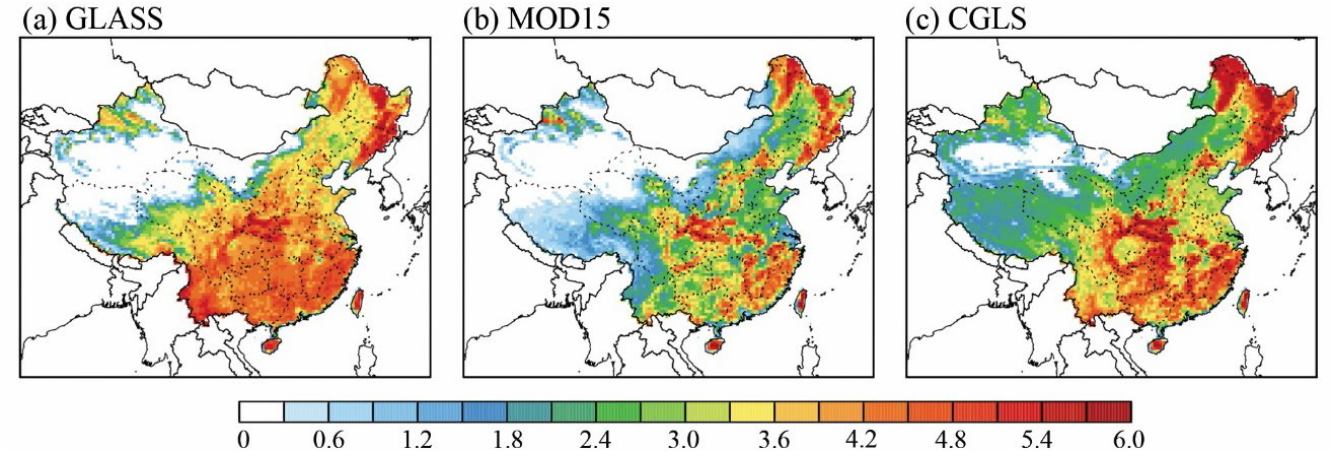

Figure 2. Distribution of LAIv from different satellite datasets in the summer of 2016.

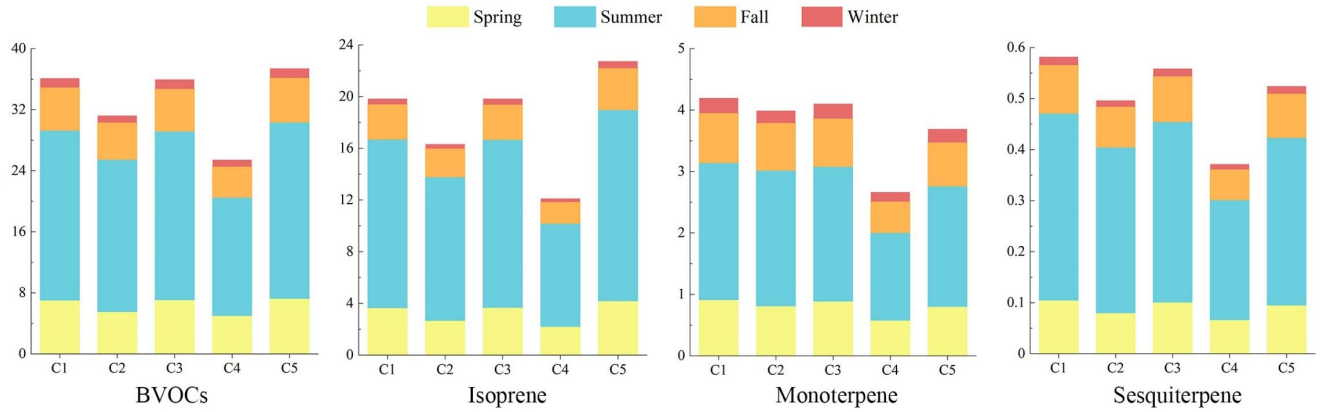

585

Figure 3. Seasonal emissions of isoprene, monoterpenes, sesquiterpenes, and total BVOCs of each case in China. Unit is Tg.

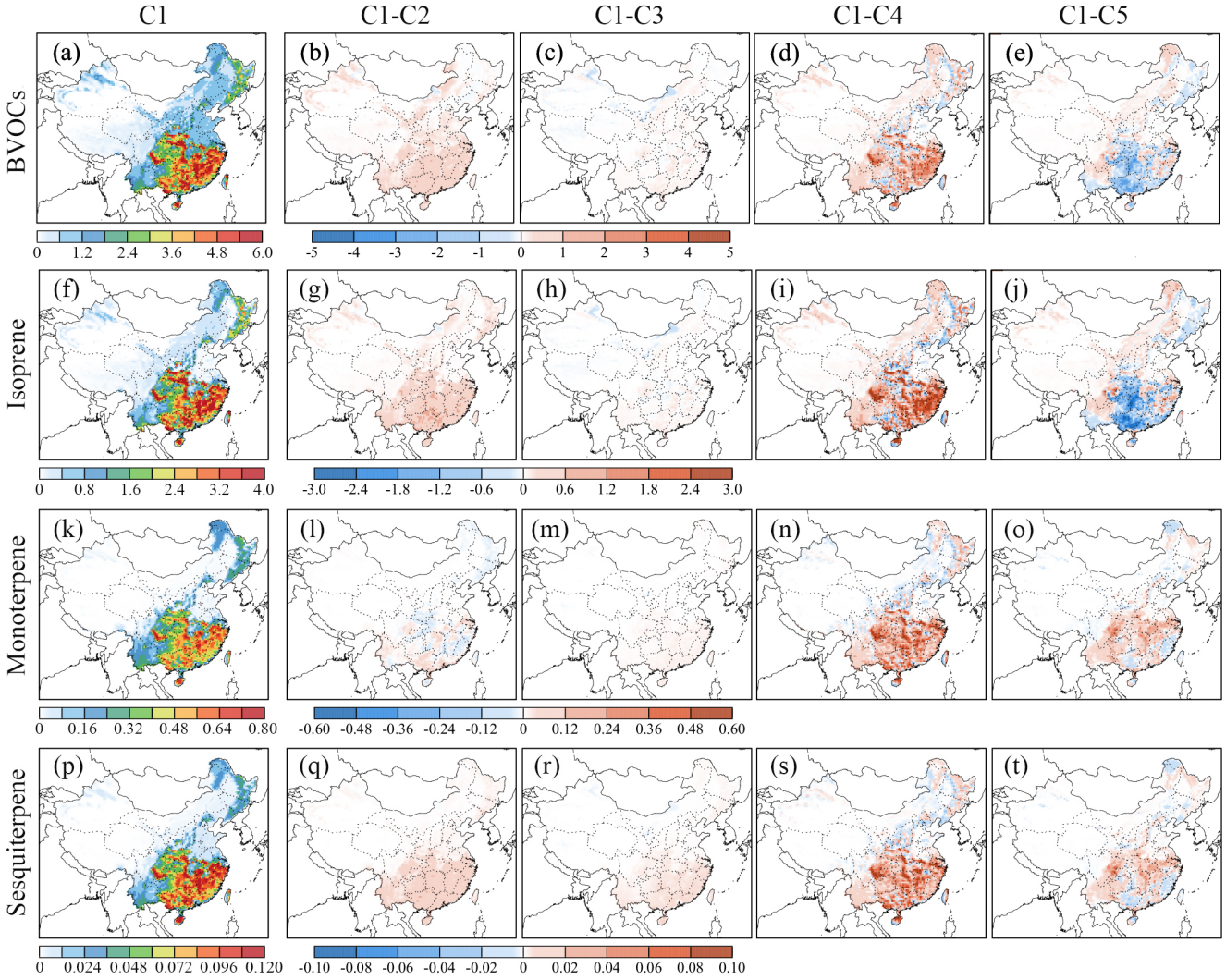

Figure 4. Comparison of three main BVOC species in different cases in summer (June, July and August) ((a), (f), (k), and (p): C1; (b), (g), (l), and (q): C1-C2; (c), (h), (m), and (r): C1-C3; (d), (i), (n), and (s): C1-C4; (e), (j), (o), and (t): C1 -C5). Unit is mg m^{-2} h^{-1}.

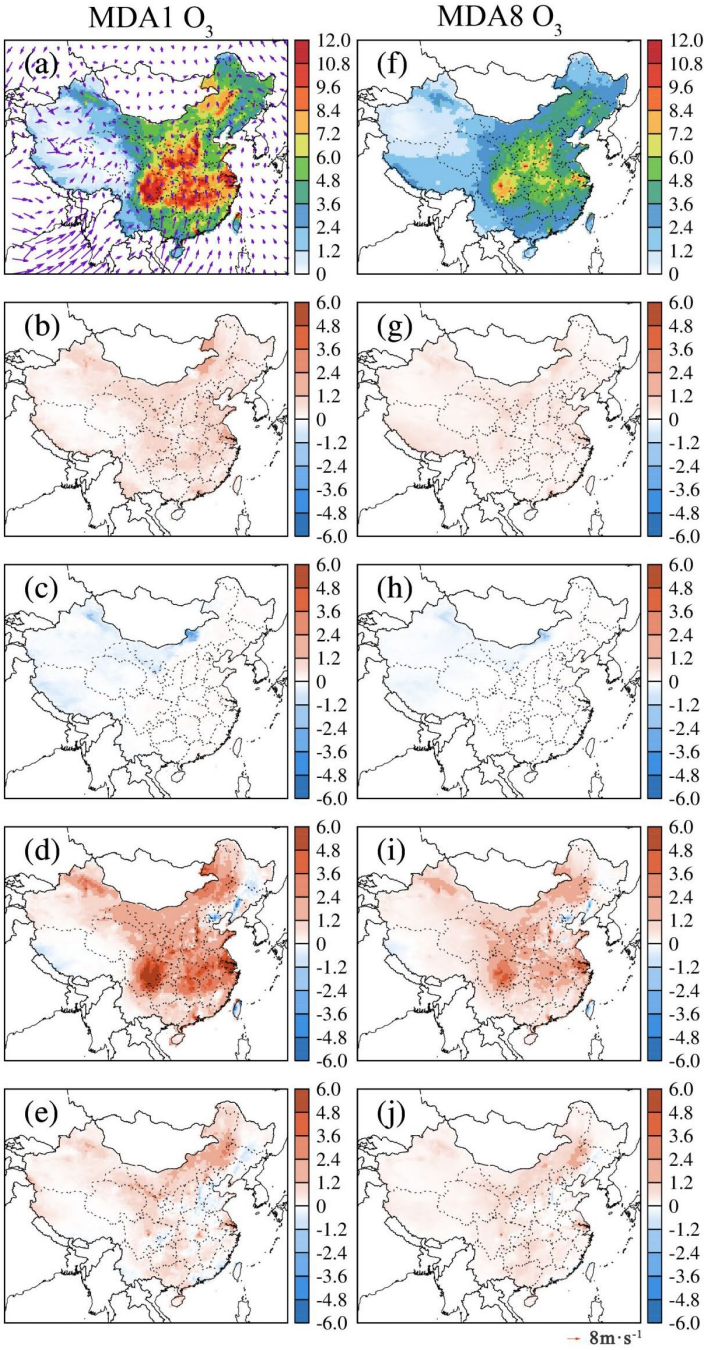

Figure 5. Spatial distributions of MDA1 O_3 and MDA8 O_3 from biogenic source in different cases in summer ((a) and (f): C1, (b) and (g): C1-C2, (c) and (h): C1-C3, (d) and (i): C1-C4, (e) and (j): C1-C5). Unit is ppb.

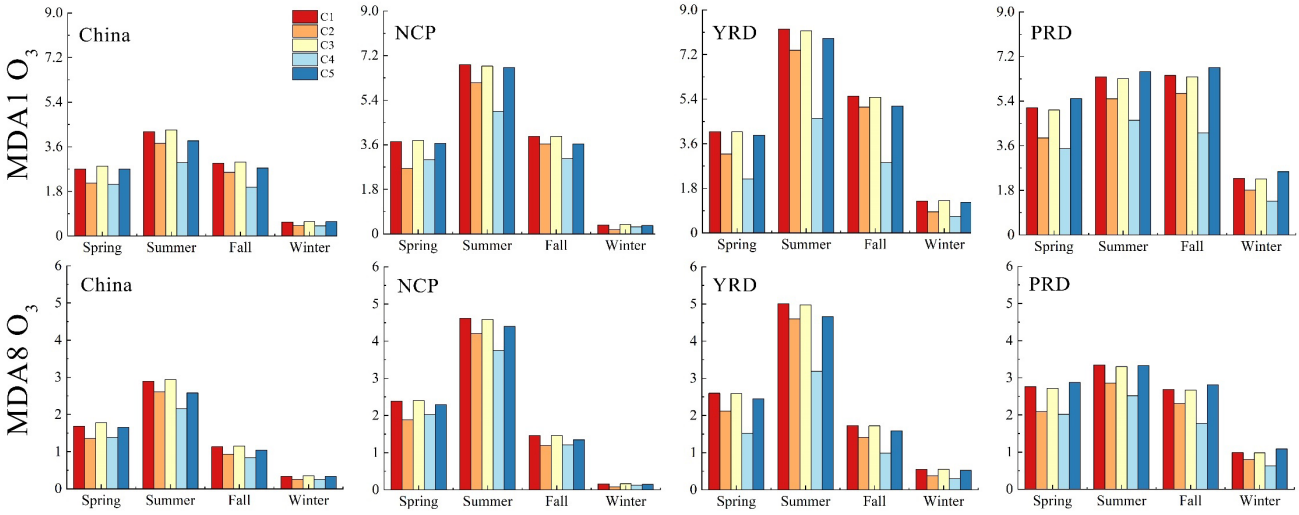

Figure 6. Seasonal averaged concentrations of MDA1 O_3 and MDA8 O_3 from biogenic emissions in important regions and China.

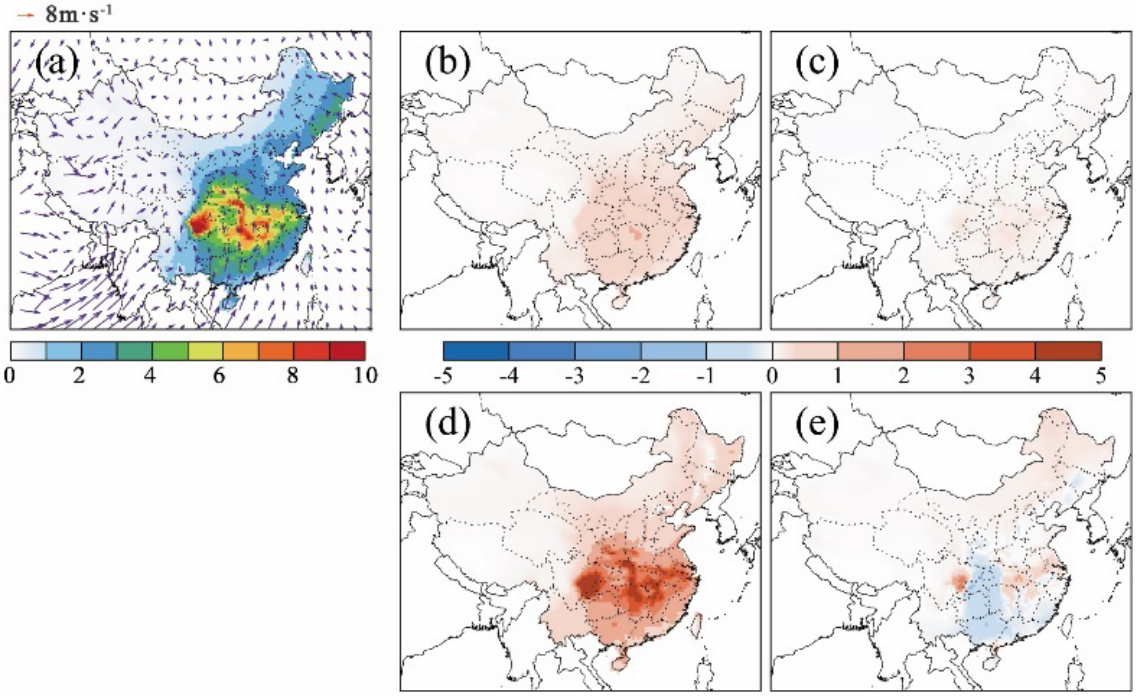

600

Figure 7. Spatial distributions of simulated SOA from biogenic source in different cases in summer. Unit is μg m^{-3} ((a): C1, (b): C1-C2, (c): C1-C3, (d): C1-C4, (e): C1-C5).

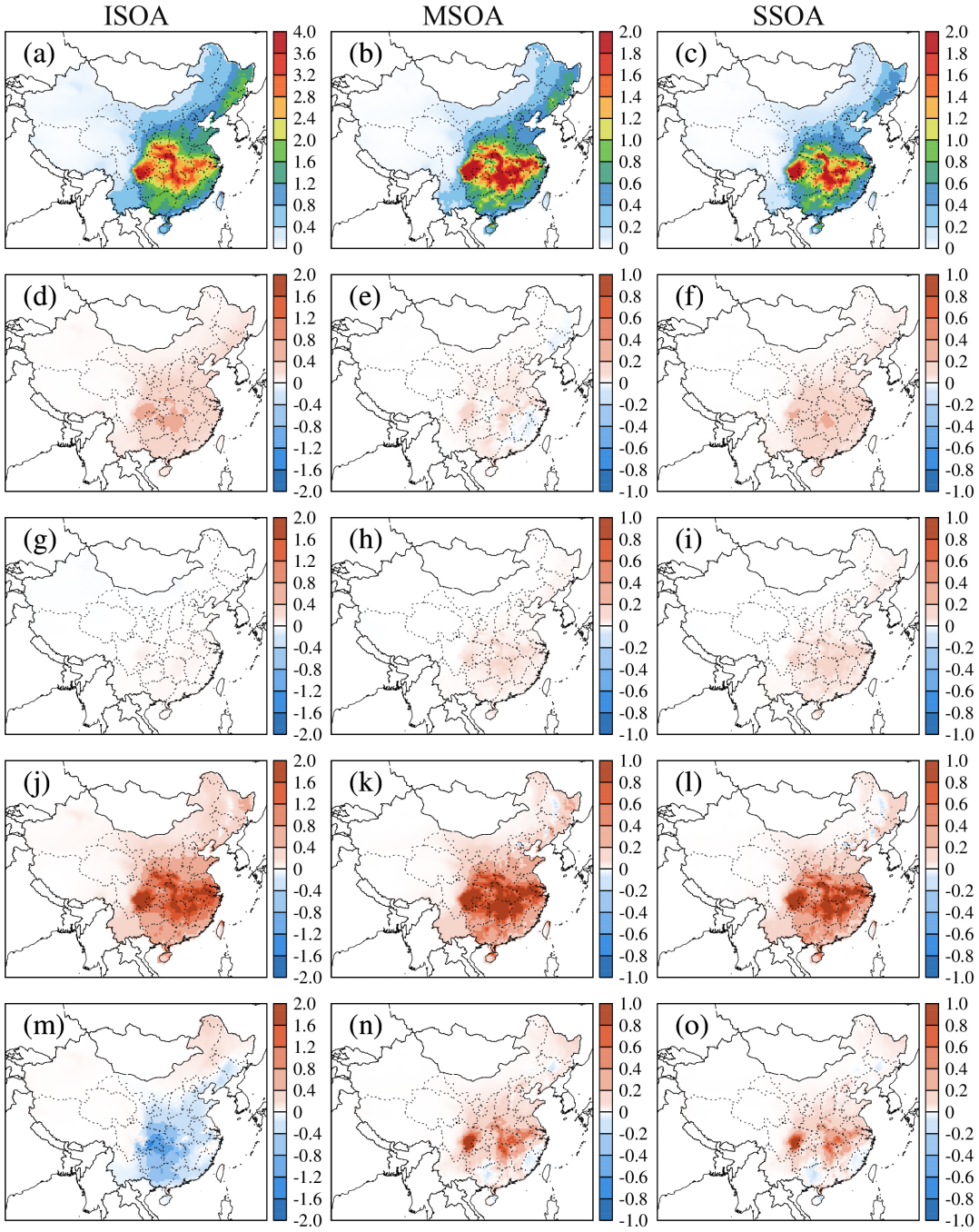

Figure 8. Spatial distributions of simulated SOA from isoprene (ISOA), monoterpenes (MSOA), and sesquiterpenes (SSOA) in different cases in summer ((a), (b), and (c): C1; (d), (e), and (f): C1-C2; (g), (h), and (i): C1-C3; (j), (k), and (l): C1-C4; (m), (n), and (o): C1-C5). Unit is μg m^{-3}.

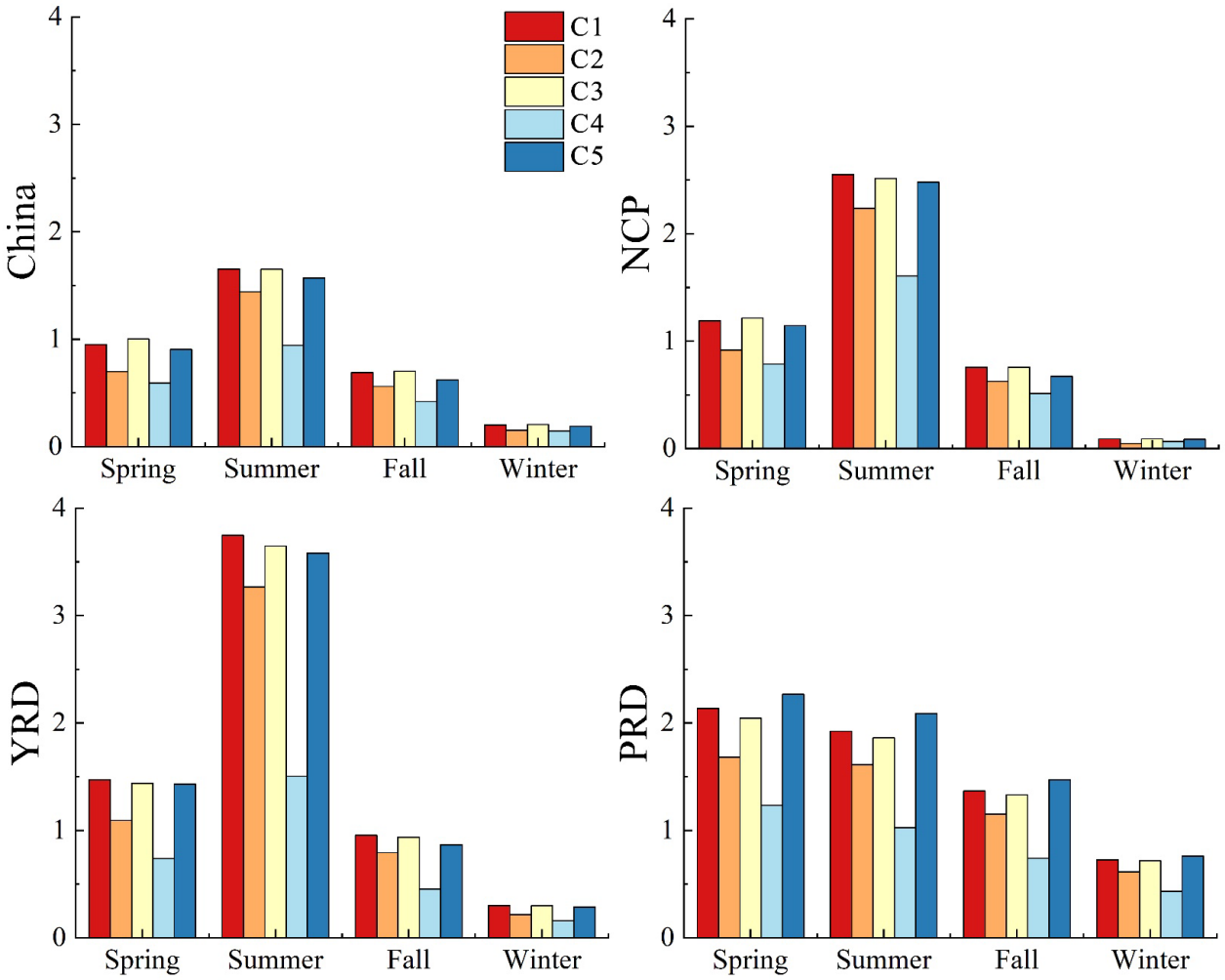

610 **Figure 9. Seasonal distributions of biogenic SOA (BSOA) for all cases in important regions and China. Unit is μg m^{-3}.**

Table 1. Simulation schemes with different land cover (LC) and leaf area index (LAI).

Case	BVOCs		Description
	LC	LAI	
C1	MCD12Q1	GLASS	As baseline
C2	MCD12Q1	MOD15	Compared to C1, accounts for LAI difference between GLASS and MOD15
C3	MCD12Q1	CGLS	Compared to C1, accounts for LAI difference between GLASS and CGLS
C4	C3S LC	GLASS	Compared to C1, accounts for LC difference between MCD12Q1 and C3S LC
C5	CGLS LC	GLASS	Compared to C1, accounts for LC difference between MCD12Q1 and CGLS LC

615 **Table 2. Estimated BVOC emissions (Tg) in different cases across China.**

	C1	C2	C3	C4	C5
Isoprene	19.84	16.32	19.83	12.10	22.73
Monoterpenes	4.19	3.99	4.10	2.66	3.69
Sesquiterpenes	0.58	0.50	0.56	0.37	0.52
Other BVOCs	11.49	10.42	11.46	10.29	10.45
Total	36.10	31.22	35.94	25.42	37.39

Table 3. Previous studies of BVOC emissions estimated using MEGAN in China, unit is Tg yr^{-1}.

Reference	Year	LAI	PFT	Isoprene	Monoterpenes	Total BVOCs
Wang et al. (2021)	2016	MODIS MOD15A2H	MODIS MCD12C1	16.70	4.12	35.48
Wu et al. (2020)	2017	MODIS MOD15A2H	MODIS MCD12Q1	13.30	3.09	23.54
Li et al. (2020)	2018	MEGAN-L database	Vegetation Atlas	37.45	6.69	58.89
Stavrakou et al. (2014)	1979-2012	MODIS MOD15A2H	Default MEGAN map with the updated cropland map	9.30	\	\
Li et al. (2013)	2003	Biomass-apportion models results	Vegetation Atlas	20.70	4.90	42.50
Fu and Liao (2012)	2001-2006	MODIS MOD15A2H	MODIS MCD12Q1	9.59	2.83	18.85